Journal of Materials Chemistry A

Accepted Manuscript

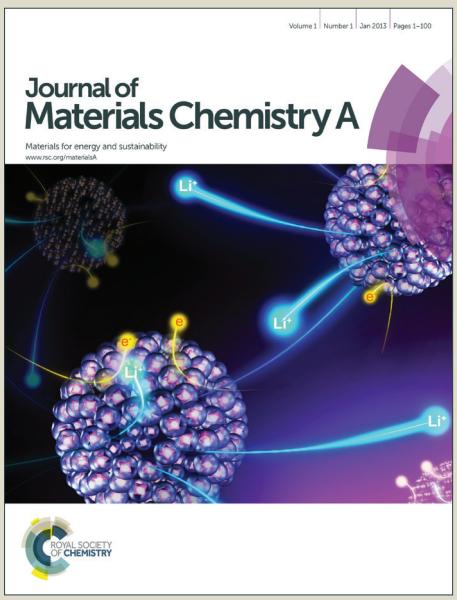

ROYAL SOCIETY OF CHEMISTRY

www.rsc.org/materialsA

Journal of Materials Chemistry A RSCPublishing

ARTICLE

A novel graphene sheet-wrapped $Co_2(OH)_3Cl$ composite as a long-life anode material for lithium ion batteries

Cite this: DOI: 10.1039/xoxxoooooox

Received ooth January 2012,
Accepted ooth January 2012

DOI: 10.1039/xoxxoooooox

www.rsc.org/

Jingjing Ma,[a] Tao Yuan,[ab] Yu-Shi He,*[a] Jiulin Wang,[a] Weimin Zhang,[ab] Dezhi Yang,[a] Xiao-Zhen Liao,[a] and Zi-Feng Ma*[ac]

A novel graphene sheet-wrapped cobalt hydroxide chloride composite ($Co_2(OH)_3Cl$@GS) is synthesized by a facile one-pot and *in situ* growth, hydrothermal method, which presents dramatically improved cycling stability and rate capability for long-life lithium ion battery. These exceptional performances are ascribed to the introduction of chlorine group and the extraordinary synergistic effect between $Co_2(OH)_3Cl$ and GS.

Introduction

Li-ion batteries (LIBs) have been considered as one of the main power sources for portable electronics and electric vehicles owing to their various advantages, such as relatively low cost, high energy density and long cycle life.[1] However, the conventional electrode materials are difficult to meet the ever-increasing demands because of their inherent limits in performance.[2] For this reason, there have been tremendous efforts reported to explore and develop high-performance electrode materials which possess the potentiality to efficiently store and deliver more energy for LIBs.[3, 4]

Cobalt hydroxide, as an important functional inorganic material, has been found its applications in the field of catalysis,[5] magnetic materials,[6] and electrochemical supercapacitors.[7, 8] Recently, since $Co(OH)_2$ was firstly reported as an anode material for LIBs by our group in 2010,[9] metal hydroxide-based materials have attracted researchers' attention owing to their high lithium storage capacity.[10-13] Nevertheless, the rate and cycling performance of the metal hydroxide-based materials cannot be satisfactory even after coating with graphene.[11] Furthermore, researches have confirmed that electrochemically reversibly reaction with lithium *via* conversion reactions can be extended to metal chlorides.[14, 15] Especially $CoCl_2$ has been found exhibiting particular high cycling performance and good rate capability.[14] It can even deliver a reversible capacity of about 300 mAh g^{-1} at 1 C rate after 50 cycles. Therefore, a cobalt-based composite can be designed by simultaneously incorporating both the chlorine and hydroxyl functional groups, and expected to result in a superior electrochemical performance especially for high rate and cycling capabilities. $Co_2(OH)_3Cl$, which has a pyrochlore-like crystal structure with a space group of R3m and consists of slightly distorted corner-sharing tetrahedrons,[16] is one of the compounds which may meet the requirements mentioned above. Besides, as an interesting magnetic geometrically frustrated material with specific properties of coexistence of ferromagnetic order and disorder, $Co_2(OH)_3Cl$ has been studied for several years and recently shown to be a material closely related to the spin ice.[17, 18] To the best of our knowledge, there are no reports about $Co_2(OH)_3Cl$ as an electrochemical material. Nonetheless, in order to effectively improve the electrical conductivity of $Co_2(OH)_3Cl$, the introduction of conductive carbon-based materials, such as graphene, is very necessary.

Graphene, a recently discovered carbonaceous material possessing a range of extraordinary properties, has attracted worldwide attention in many fields including energy storage materials.[19-22] The principal issue in the synthesis of the graphene-based composites presently focuses on how to effectively prevent the graphene sheets from agglomeration and restacking in the preparation process to fully harness the unique properties of individual graphene sheet and adequately utilize the synergistic effect between graphene sheets and the other component.[23, 24]

Herein, we firstly reported a graphene sheet-encapsulated $Co_2(OH)_3Cl$ composite ($Co_2(OH)_3Cl$@GS) as an advanced anode material for LIBs using a simple and one-pot *in situ* growth hydrothermal method. The $Co_2(OH)_3Cl$ particles was synthesized *via in situ* growth on the surfaces of the GS which effectively prevented the restacking of GS. Comparing with the bare $Co_2(OH)_3Cl$, the $Co_2(OH)_3Cl$@GS composite exhibited remarkably improved cycling stability and rate capability at room and high temperature.

Experimental details

Synthesis of $Co_2(OH)_3Cl$@GS

Graphite oxide was synthesized from natural graphite powder (Grade 230, Asbury Carbons) by a modified Hummer's method. The graphite oxide (20 mg) was exfoliated into 10 mL deionized water by sonication to form a graphene oxide (GO) suspension. Then, 0.8 mmol of $CoCl_2 \cdot 6H_2O$, 0.8 mmol NaOH and 0.8 mmol Dodecylamine (DDA) were added into the above solution. The mixture was put in a Teflon-lined autoclave and maintained the temperature at 180 °C for 12 h. After naturally cooling down to room temperature, a black columniform product was obtained and washed by ethanol and water to remove the residual DDA and ions. Pure $Co_2(OH)_3Cl$ sample was also prepared by the same procedure for comparison. All as-prepared samples were freeze-dried for the following tests.

Structural and morphological characterization

X-ray diffraction (XRD) measurements were performed on a Rigaku D/MAX-2200/PC X-ray diffractometer at 40 kV and 20 mA, with a Cu Kα radiation source. X-ray photoelectron spectrometer (XPS, Kratos Axis Ultra DLD) was used to examine the surface chemistry of the samples. Thermogravimetric analysis (TGA) was conducted using a STA 449F3 analyzer (NETZSCH Co., Germany) to determine the residual level of $Co_2(OH)_3Cl$@GS after calcination. Raman spectroscopy was utilized to characterize of the samples *via* using a Bruker Optic SENTERRA (R-200L) with the laser wavelength of 532 nm at room temperature. The morphology and microstructure of the samples were investigated by a FEI Nova SEM 230 ultra-high resolution field emission scanning electron microscopy (FESEM) equipped with energy dispersive X-ray spectroscopy (EDS, INCA X-Max 80, Oxford Instruments). Transmission election microscopy (TEM) was operated with JEM-2010.

Electrochemical measurements

The samples ($Co_2(OH)_3Cl$@GS and $Co_2(OH)_3Cl$) were dried at 80 °C for 3h in an Ar atmosphere. The working electrodes were formed by mixing 75 wt% active material ($Co_2(OH)_3Cl$@GS or $Co_2(OH)_3Cl$), 15 wt% acetylene black (Super-P), and 10 wt% polyvinylidene fluoride (PVDF) binder and coating the slurry onto Cu foil disks. The electrodes were dried, cut to Φ14 mm sheets, pressed at 3 MPa, and finally dried at 80 °C under vacuum for 4 h to remove the residual solvent. The mass loading of active material on each electrode was about 1 $mg \cdot cm^{-2}$. Electrochemical experiments were carried out in CR2016 coin cells. The cells were assembled in an argon-filled glove box with pure lithium foil as counter electrode and UP3025 separator (UBE, Japan). The electrolyte contained 1 M $LiPF_6$ in dimethyl carbonate (DMC) and ethylene carbonate (EC) mixed solvent of 1:1 (v/v, LP30). Charge–discharge cycles of the half-cells were evaluated between 0.005 and 3 V vs Li/Li^+ at room temperature using LAND CT2001A model battery test system (Wuhan Jinnuo, China) under constant current condition. The charge-discharge capacities were calculated according to the weight of active materials in the electrode. Cyclic voltammetry (CV) measurements were performed by using a CHI instrument (CHI 660) potentiostat with a scan rate of 0.1 mV s^{-1}. The AC electrochemical impedance spectra (EIS) tests of the cells were measured using a three-electrode system (MTI Corporation) and recorded using a Autolab PGSTAT302N (Metrohm) model electrochemical workstation with an amplitude of 10 mV over a frequency range from 100 kHz to 0.1 Hz. The three-electrode system consists of a $Co_2(OH)_3Cl$@GS working electrode, a lithium foil counter and a lithium ring reference electrode.

Results and discussion

The overall preparation process of self-assembled three-dimensional (3D) $Co_2(OH)_3Cl$@GS composite is shown in Fig. 1. First, the as-prepared graphite oxide is sonicated in deionized water to yield a uniform yellow–brown dispersion of GO (Fig. 1a). Second, $CoCl_2 \cdot 6H_2O$ is added into above solution and sonicated with GO to form an opaque and dark-red dispersion (Fig. 2b). The oxygen-containing functional groups on GO surfaces/edges with negative charge can then bind with Co^{2+} ions by electrostatic interactions and act as fixed reaction sites. After NaOH and DDA (Dodecylamine) are successively added into above dispersion, the obtained mixture is self-assembled under hydrothermal condition at 180 °C for 12 h, thus forming a dark-green columniform hydrogel of $Co_2(OH)_3Cl$@GS after removing the residual DDA and other ions by washing with ethanol and water. During the hydrothermal process, the *in situ* nucleation and growth of $Co_2(OH)_3Cl$ crystals adsorbed on GO sheets are simultaneous with the reduction of GO and the self-assembly of GS framework. Finally, the as-obtained $Co_2(OH)_3Cl$@GS hydrogel is freeze-dried to obtain the 3D $Co_2(OH)_3Cl$@GS aerogel.

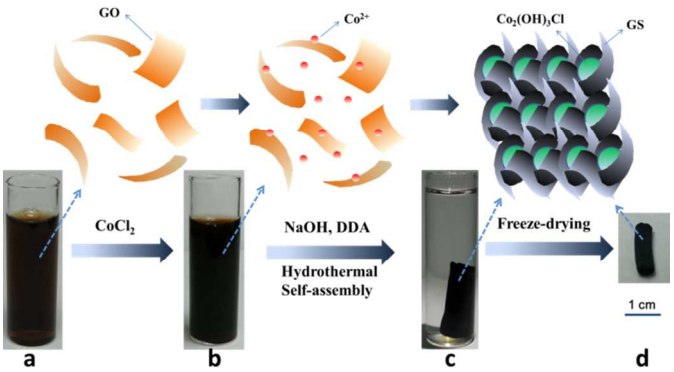

Fig. 1. Preparation process of self-assembled 3D $Co_2(OH)_3Cl$@GS composite: a) uniform yellow–brown dispersion of GO in deionized water; b) homogeneous and opaque black dispersion of GO and $CoCl_2 \cdot 6H_2O$; c) $Co_2(OH)_3Cl$@GS hybrid hydrogel synthesized by hydrothermal self-assembly; d) $Co_2(OH)_3Cl$@GS hybrid aerogel obtained after freeze-drying.

Fig. 2a show the XRD patterns of as-prepared $Co_2(OH)_3Cl$@GS and bare $Co_2(OH)_3Cl$. For the two samples, the major diffraction peaks of (101), (113), (024), and (220) match well with those of the standard rhombohedral $Co_2(OH)_3Cl$ (JCPDS 73-2134). No clear characteristic peak of GO at about 11° is detected for the $Co_2(OH)_3Cl$@GS composite, indicating that GO has been simultaneously reduced into GS during the hydrothermal process. Additionally, we did not observe the characteristic (002) stacking peak of graphene at about 20−30°, which suggests that $Co_2(OH)_3Cl$ particles effectively grow on the surface of GS and successfully inhibit the restacking of GS.[23, 25] It is noteworthy that the diffraction peaks of $Co_2(OH)_3Cl$@GS composite is sharper than those of pure $Co_2(OH)_3Cl$ sample, which can be attributed that the presence of the oxygen-containing functional groups (hydroxyl, carboxyl and epoxy etc.) on GO improves the crystallization of $Co_2(OH)_3Cl$. The as-obtained materials were further examined by Raman spectra. As shown in Fig. S1†, two characteristic broad peaks are quite visible at about 1340 and 1597 cm^{-1} which can be assigned to the disordered D band and the graphitic G band of carbon materials, respectively. And the intensity ratio of D to G band (I_D: I_G) of $Co_2(OH)_3Cl$@GS is clearly higher than that of GO, demonstrating that GO has been effectively reduced and a large number of structure defects have been introduced due to the interfacial interaction between the graphitic plane and $Co_2(OH)_3Cl$.[26, 27]

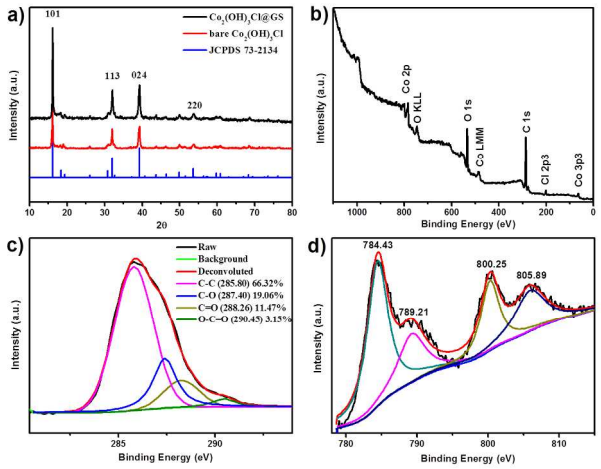

Fig. 2. (a) XRD patterns for the $Co_2(OH)_3Cl$@GS and bare $Co_2(OH)_3Cl$. (b-d) XPS spectra for the $Co_2(OH)_3Cl$@GS composite: (b) survey spectrum and high-resolution (c) C 1s and (d) Co 2p spectra.

XPS analysis can provide important information on the surface chemical composition and electronic state of the $Co_2(OH)_3Cl$@GS composite. The survey XPS spectrum for the composite was shown in Fig. 2b, indicating the existence of C, O, Co, and Cl elements.[28] In Fig. 2c, the C1s XPS spectrum of $Co_2(OH)_3Cl$@GS composite was used to assess the reduction degree of GO produced by the hydrothermal treatment. In Fig. 2c, there are four different peaks which are associated with carbon sp^2 (C-C, ~285.80 eV), epoxy/hydroxyl groups (C-O, ~287.40 eV), carbonyl group (C=O, ~288.26 eV), and carboxyl group (O-C=O, ~290.45 eV), respectively.[24] The fraction of carbon-carbon bonding is about 66.32%, which can be attributed specifically to the removal of oxygen-containing functional groups from the GO by the hydrothermal process and reveal the formation of graphene.[29] Fig. 2d exhibits the high-resolution Co 2p spectrum of the composite. The two major peaks at 784.43 and 800.25 eV correspond respectively to the characteristic peaks of Co 2p 3/2 and Co 2p 1/2 for $Co_2(OH)_3Cl$, while two weak peaks at 789.21 and 805.89 eV belong to the shake-up satellite peaks of above two peaks, demonstrating the presence of Co(II).[25]

TGA measurement tested from 35 °C to 750 °C in air was adopted to quantify the amount of graphene in the $Co_2(OH)_3Cl$@GS composite. As shown in Fig. S2†, there was a slight mass loss (about 2.4 wt %) between 35~250 °C, which can be attributed to the evaporation of water absorbed on the sample. Moreover, the significant weight loss between 250~550 °C could be ascribed to the combustion and oxidation of the $Co_2(OH)_3Cl$@GS composite.[30] The inset in Fig. S2† shows the XRD result of the calcination product of $Co_2(OH)_3Cl$@GS at 550 °C was Co_3O_4, and all the peaks can be assigned to Co_3O_4 (JCPDS No. 42-1467). The weight of Co element in the composite should keep constant during the thermal treatment, so the weight fractions of $Co_2(OH)_3Cl$ in the composite was calculated to be about 84.0 wt %. Accordingly the graphene content is determined to be about 13.6 wt %.

A field emission scanning electron microscopy (FESEM) was employed to reveal the morphologies of bare $Co_2(OH)_3Cl$ and $Co_2(OH)_3Cl$@GS. The FESEM images of the bare $Co_2(OH)_3Cl$ (Fig. 3a and 3b) demonstrate irregular secondary particles about 200-500 nm in diameter with a stacking lamellar structure. Fig. 3c and 3d show that the $Co_2(OH)_3Cl$ particles in the $Co_2(OH)_3Cl$@GS composite were evenly and tightly anchored into the graphene matrix, implying the successful self-assembly between the GS and the $Co_2(OH)_3Cl$ particles during the hydrothermal process. Furthermore, no obvious porous structure can be found in the $Co_2(OH)_3Cl$@GS composite, possibly because the graphene sheets are intertwined closely with each other during the hydrothermal treatment. Fig. S3 † shows the SEM image of the $Co_2(OH)_3Cl$@GS composite and the corresponding energy dispersive X-ray spectroscopy (EDS) mappings over a relatively large area (about 10 μm × 14 μm) for the carbon, oxygen, cobalt and chloride elements, indicating that the $Co_2(OH)_3Cl$ particles well distributed throughout the GS matrix. Microstructure of $Co_2(OH)_3Cl$@GS was further investigated by transmission election microscopy (TEM) (Fig. 3e) and high-resolution TEM (HRTEM) (Fig. 3f). As shown in Fig. 3e, the irregular $Co_2(OH)_3Cl$ particles with rough surfaces were well encapsulated by the GS and are distributed evenly in the GS framework, in consistent with the above SEM results. The HRTEM image of the $Co_2(OH)_3Cl$@GS composite, shown in Fig. 3f, demonstrates that the $Co_2(OH)_3Cl$ particle was wrapped by the multiple overlapping graphene sheets. Moreover, the well-ordered lattice fringes with a spacing of 0.28 nm can be assigned to the (113) plane of $Co_2(OH)_3Cl$.

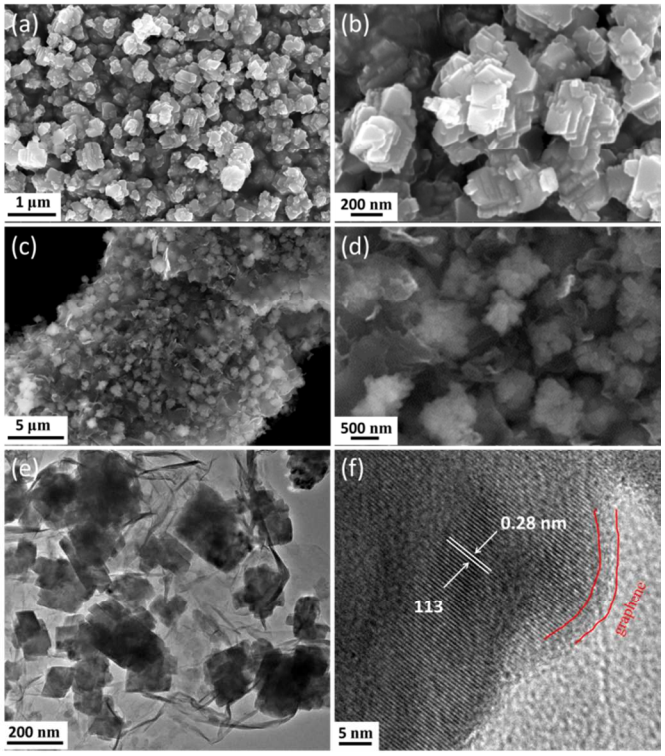

Fig. 3. Typical FESEM images of (a, b) bare $Co_2(OH)_3Cl$ and (c, d) $Co_2(OH)_3Cl$@GS composite; (e) TEM and (f) HRTEM images of $Co_2(OH)_3Cl$@GS composite.

As illustrated in Fig. 4, the electrochemical properties of as-prepared samples were evaluated by using various electrochemical measurements. Cyclic voltammetry (CV) profiles of the $Co_2(OH)_3Cl$@GS were measured to explore the kinetics of the electrochemical reactions at a scan rate of 0.1 mV s^{-1} for the first, third and tenth cycles in Fig. 4a. In the first cycle, one dominant peak and one inconspicuous peak in the cathodic polarization process can be observed at around 0.74 V and 1.24 V, respectively. The main peak at 0.74 V might arise from the formation of LiOH and solid electrolyte interphase (SEI) films.[10-13] The weak peak at around 1.24 V can be due to the formation of LiCl.[14, 31] Meanwhile, the oxidation peak at about 1.5 V in the anodic process corresponds to the reversible oxidation of cobalt to cobalt oxide.[32, 33] It is noteworthy that the CV curves show good reproducibility from the third to the tenth cycle, indicating good reversible reactions. For comparison, the CV curves of the bare $Co_2(OH)_3Cl$ were displayed in Fig. S4†, and the cathodic/anodic peaks are similar to those of $Co_2(OH)_3Cl$@GS. However, the peak current and the integrated area of the $Co_2(OH)_3Cl$ decreased gradually with the increase of cycle number, suggesting the inferior reversibility of the electrochemical reaction and the poor cycling stability. Combined with our previous research about $Co(OH)_2$ and other studies about $CoCl_2$ and PbOHCl for LIBs,[9, 14, 31] the possible electrochemical reaction mechanism of $Co_2(OH)_3Cl$@GS with Li was proposed as follows:

$$Co_2(OH)_3Cl + 4Li^+ + 4e^- \rightarrow 2Co + 3LiOH + LiCl \quad (1)$$

$$2Co + 3LiOH + LiCl \leftrightarrow \frac{1}{2}CoCl_2 + \frac{3}{2}Co(OH)_2 + 4Li^+ + 4e^- \quad (2)$$

$$6C + Li^+ + e^- \leftrightarrow LiC_6 \quad (3)$$

Based on the above reaction mechanism, the theoretical capacity of $Co_2(OH)_3Cl$ was calculated as 525 mAh g^{-1} with a maximum 4 Li uptake per formula.

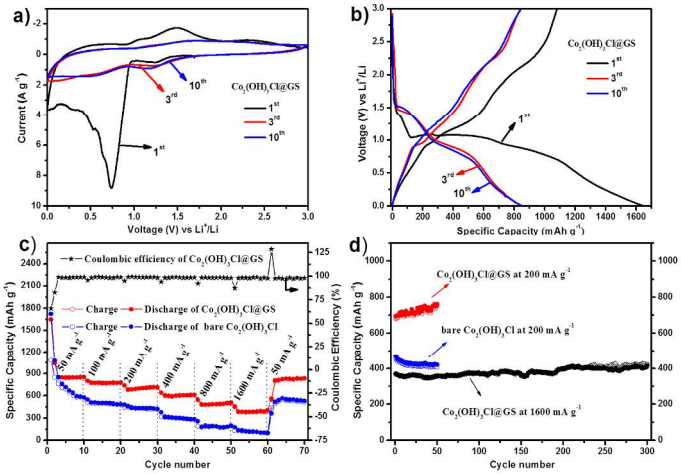

Fig. 4. (a) CV curves of the $Co_2(OH)_3Cl$@GS composite in the potential range of 0.005–3 V at a scan rate of 0.1 mV s^{-1}. (b) Charge–discharge curves of the $Co_2(OH)_3Cl$@GS composite at a current density of 50 mA g^{-1}. (c) Rate capability of the $Co_2(OH)_3Cl$@GS composite and bare $Co_2(OH)_3Cl$ at the current densities between 50 and 1600 mA g^{-1}. (d) Cycling behavior of the $Co_2(OH)_3Cl$@GS and bare $Co_2(OH)_3Cl$. Solid and hollow point symbols represent lithium insertion and extraction, respectively.

The charge (delithiation) and discharge (lithiation) of the $Co_2(OH)_3Cl$@GS composite as the anode were investigated in the voltage range of 0.005-3 V vs. Li/Li^+ at a current density of 50 mA g^{-1} at room temperature in Fig. 4b. An extended voltage plateau at about 1.1 V was evident in the first discharge process, demonstrating the SEI layer formation and the conversion reaction. The reversible capacity (around 840 mAh g^{-1}) of the $Co_2(OH)_3Cl$@GS is much higher than the theoretical capacity of $Co_2(OH)_3Cl$ (525 mAh g^{-1}). It may be ascribed to the following several aspects. First, the obvious extra capacity may be derived from the reversible formation and dissolution of polymeric gel-like film along with the discharge and charge process, respectively.[34, 35] The reversible gel-like film is part of SEI components consisting of diverse inorganic and organic salts. Second, extra lithium-ion adsorption/desorption on the SEI while cycling may also lead to the high experimental lithium storage capacity.[34, 36] Besides, the graphene nanosheets have significant disorder/defects and oxygenated functional groups on the surface of the graphene in the $Co_2(OH)_3Cl$@GS can be reduced during cycling, which can also contribute to the lithium storage capacity, in addition to the intrinsic theoretical capacity.[32, 37] The initial Coulombic efficiency (CE) of the $Co_2(OH)_3Cl$@GS is around 66%, which is close to that of the bare $Co_2(OH)_3Cl$ (63%) (Fig. S5†). And the CE increases

quickly to nearly 99% since the third cycle, which is in good agreement with the CV results. Moreover, for the $Co_2(OH)_3Cl$@GS electrode, no distinct capacity loss was found after 2 cycles, and the reversible capacity still remained at around 840 mAh g^{-1} after 10 cycles. In contrast, the reversible capacity of the $Co_2(OH)_3Cl$ electrode gradually decreased to approximately 570 mAh g^{-1} at tenth cycle. Fig. 4c depicts the rate capability of bare $Co_2(OH)_3Cl$ and $Co_2(OH)_3Cl$@GS from current densities of 50 to 1600 mA g^{-1}. As expected, the $Co_2(OH)_3Cl$@GS electrode manifested a remarkable rate performance compared to the bare $Co_2(OH)_3Cl$. Even at a high charge/discharge current density of 1600 mA g^{-1}, the $Co_2(OH)_3Cl$@GS electrode still exhibited a favorable reversible capacity of 397 mAh g^{-1}, while the $Co_2(OH)_3Cl$ only delivered a reversible capacity of 130 mAh g^{-1}. More importantly, when the current density was returned to 50 mA g^{-1}, the $Co_2(OH)_3Cl$@GS electrode recovered to a high reversible capacity, denoting the stable structure of the $Co_2(OH)_3Cl$@GS composite and good reversibility. The cycling performance of the $Co_2(OH)_3Cl$@GS was further probed in Fig. 4d. All cells were cycled at a current density of 50 mA g^{-1} for the initial two cycles before each test. The cycling performance of the $Co_2(OH)_3Cl$@GS is superior to that of the bare $Co_2(OH)_3Cl$. At a current density of 200 mA g^{-1}, the reversible capacity gradually increased to 753 mAh g^{-1} after 50 cycles. The upward trend of capacity with the cycles may be assigned to the reversible growth of the polymeric gel-like film deriving from the kinetically activated electrolyte degradation[34, 38] or the interfacial Li storage.[39, 40] Similar phenomena have also been widely observed in other metal oxide/graphene composites.[32, 41-43] The reversible capacity of the bare $Co_2(OH)_3Cl$ electrode, by contrast, gradually decreased and only maintained at 407 mAh g^{-1} after 50 cycles. In addition, the $Co_2(OH)_3Cl$@GS composite possesses extraordinary high-rate cycling performance, which can still deliver a reversible capacity of 414 mAh g^{-1} after 300 cycles even at a high current density of 1600 mAh g^{-1}. So as to further illustrate the effect of the introduction of chlorine group on the electrochemical performance of the composite, the rate and cycling capability of bare $Co_2(OH)_3Cl$ and $Co_2(OH)_3Cl$@GS composite synthesized in this work and those of $Co(OH)_2$ and $Co(OH)_2$-based composites reported in the literatures[9-11] are summarized in the Table S1†. Obviously, the presence of chlorine group greatly reinforces the electrochemical performance of the composites. Furthermore, Fig. S6 † exhibits that the $Co_2(OH)_3Cl$@GS electrode manifested excellent high-rate cycling stability at high temperature (55 ^oC) at a discharge/discharge current density of 1600 mAh g^{-1}. Evidently, the cycling performance and reversible capacity of the $Co_2(OH)_3Cl$@GS are much better than that of the bare $Co_2(OH)_3Cl$. After 100 cycles, the $Co_2(OH)_3Cl$@GS electrode still displayed a high reversible capacity of 701 mAh g^{-1}, while the bare $Co_2(OH)_3Cl$ electrode showed a reversible capacity of only 207 mAh g^{-1}. The exceptional performance could be assigned to the special flexibility of GS which made the electrode more insensitive to the mechanical stresses undergone during the cycling process at high temperature and high-rate.

In order to further clarify the improved electrochemical performance after introducing the graphene into the $Co_2(OH)_3Cl$@GS composite, electrochemical impedance spectra for the bare $Co_2(OH)_3Cl$ and $Co_2(OH)_3Cl$@GS composite were collected with a three-electrode system after 50 cycles at a current density of 200 mAh g^{-1} (Fig. S7†). To maintain uniformity, electrochemical impedance spectroscopy (EIS) was performed on the working electrodes in the fully charged (delithiated) state. The depressed semicircle in the high-medium frequency region is related to the capacitance of the electrode interface, while the inclined line in the low frequency range represents the Warburg impedance, which corresponds to solid-state diffusion of Li ions within the electrodes.[21] The depressed semicircle arc for the $Co_2(OH)_3Cl$@GS electrode is much smaller than that of the bare $Co_2(OH)_3Cl$ electrode, which suggests that the $Co_2(OH)_3Cl$@GS electrode possesses lower ohmic and capacitive resistances. Moreover, the improved electronic connection and charge/discharge properties of the $Co_2(OH)_3Cl$ electrode have been achieved by effective encapsulation and adherence of highly conductive and flexible GS.

In summary, the outputs clearly illustrate the significantly enhanced cycling and rate performance of $Co_2(OH)_3Cl$@GS as a novel anode material for lithium storage. We electrochemically confirmed that the introduction of chlorine group in the composite effectively improved the cycling and rate performance of the composite. Also, we found $Co_2(OH)_3Cl$ particles were wrapped in GS matrix which intimately contacted with GS *via* the one-pot *in situ* hydrothermal route. The particles evenly anchored into the GS network acted as spacers, which effectively inhibited the restacking of GS. In addition, in the $Co_2(OH)_3Cl$@GS composite, GS with excellent flexibility not only buffered volume expansion and decreased the strain associated with the volume variation, but also provided electronic conductive channels to improve the electronic conductivity of the composite and greatly decrease the Ohmic loss.

Conclusions

We successfully synthesized a $Co_2(OH)_3Cl$@GS composite as a novel anode material for LIBs *via* a facile one-pot *in situ* hydrothermal route. In this process, the *in situ* nucleation and growth of $Co_2(OH)_3Cl$ particles on the surface of the GS occur simultaneously with the reduction and the formation of the GS network. As a consequence, electrochemical measurements indicated that the as-synthesized $Co_2(OH)_3Cl$@GS exhibits superior cycling stability and rate capability even at high temperature, owing to the introduction of the chlorine group, the unique self-assembled structure and the desirable synergistic effect between $Co_2(OH)_3Cl$ and GS.

Acknowledgements

We are grateful for financial support for this work from the National Basic Research Program of China (2014CB239700), the Natural Science Foundation of China (21336003, 21006063), China Postdoctoral Science Foundation (2013M541510) and the Natural Science Foundation of Shanghai (12DZ0502200).

Notes and references

[a] Institute of Electrochemical and Energy Technology, Department of Chemical Engineering, Shanghai Jiao Tong University, Shanghai, 200240, China; Tel: +86-21-54742894; Fax: +86-21-54741297; E-mail: ys-he@sjtu.edu.cn, zfma@sjtu.edu.cn
[b] Sinopoly Battery Research Center, Shanghai, 200241, China.
[c] Department of Chemical and Biological Engineering, Zhejiang University, Hangzhou, 310027, China

† Electronic Supplementary Information (ESI) available: [Raman spectra, XRD patterns, TGA curves, EDS mapping, charge/discharge curves, the cycling performance of the samples at high temperature, impedance plots]. See DOI: 10.1039/b000000x/

1. H. Li and H. Zhou, *Chem. Commun.*, 2012, **48**, 1201-1217.
2. L. Yu, L. Zhang, H. B. Wu, G. Zhang and X. W. Lou, *Energy Environ. Sci.*, 2013, **6**, 2664-2671.
3. P. G. Bruce, B. Scrosati and J. M. Tarascon, *Angew. Chem., Int. Ed.*, 2008, **47**, 2930-2946.
4. M. V. Reddy, G. V. Subba Rao and B. V. Chowdari, *Chem. Rev.*, 2013, **113**, 5364-5457.
5. Y. Wang, D. Zhang and H. Liu, *J. Power Sources*, 2010, **195**, 3135-3139.
6. M. Kurmoo, *Chem. Mater.*, 1999, **11**, 3370-3378.
7. V. Gupta, T. Kusahara, H. Toyama, S. Gupta and N. Miura, *Electrochem. Commun.*, 2007, **9**, 2315-2319.
8. S. Chen, J. Zhu and X. Wang, *J. Phys. Chem. C*, 2010, **114**, 11829-11834.
9. Y.-S. He, D.-W. Bai, X. Yang, J. Chen, X.-Z. Liao and Z.-F. Ma, *Electrochem. Commun.*, 2010, **12**, 570-573.
10. X.-l. Huang, X. Zhao, Z.-l. Wang, L.-m. Wang and X.-b. Zhang, *J. Mater. Chem.*, 2012, **22**, 3764-3769.
11. X.-l. Huang, J. Chai, T. Jiang, Y.-J. Wei, G. Chen, W.-q. Liu, D. Han, L. Niu, L. Wang and X.-b. Zhang, *J. Mater. Chem.*, 2012, **22**, 3404-3410.
12. S. Ni, X. Lv, T. Li, X. Yang and L. Zhang, *J. Mater. Chem. A*, 2013, **1**, 1544-1547.
13. B. Li, H. Cao, J. Shao, H. Zheng, Y. Lu, J. Yin and M. Qu, *Chem. Commun.*, 2011, **47**, 3159-3161.
14. J.-l. Liu, W.-j. Cui, C.-x. Wang and Y.-y. Xia, *Electrochem. Commun.*, 2011, **13**, 269-271.
15. T. Li, Z. X. Chen, Y. L. Cao, X. P. Ai and H. X. Yang, *Electrochim. Acta*, 2012, **68**, 202-205.
16. S. Maegawa, A. Oyamada, S. Sato, M. Nishiyama, T. Itou and X. G. Zheng, *J. Phys.: Conf. Ser.*, 2009, **145**, 012018.
17. X. Zheng, T. Kawae, H. Yamada, K. Nishiyama and C. Xu, *Phys. Rev. Lett.*, 2006, **97**, 247204.
18. X. Zheng, M. Hagihala, T. Kawae and C. Xu, *Phys. Rev. B*, 2008, **77**, 024418.
19. Y.-S. He, P. Gao, J. Chen, X. Yang, X.-Z. Liao, J. Yang and Z.-F. Ma, *RSC Adv.*, 2011, **1**, 958-960.
20. T. Yuan, W.-T. Li, W. Zhang, Y.-S. He, C. Zhang, X.-Z. Liao and Z.-F. Ma, *Ind. Eng. Chem. Res.*, 2014, **53**, 10849-10857.
21. L. Yin, J. Wang, F. Lin, J. Yang and Y. Nuli, *Energy Environ. Sci.*, 2012, **5**, 6966-6972.
22. D. Yang, X.-Z. Liao, J. Shen, Y.-S. He and Z.-F. Ma, *J. Mater. Chem. A*, 2014, **2**, 6723-6726.
23. G.-W. Zhou, J. Wang, P. Gao, X. Yang, Y.-S. He, X.-Z. Liao, J. Yang and Z.-F. Ma, *Ind. Eng. Chem. Res.*, 2013, **52**, 1197-1204.
24. J. Ma, J. Wang, Y.-S. He, X.-Z. Liao, J. Chen, J.-Z. Wang, T. Yuan and Z.-F. Ma, *J. Mater. Chem. A*, 2014, **2**, 9200-9207.
25. Y. Sun, X. Hu, W. Luo and Y. Huang, *J. Phys. Chem. C*, 2012, **116**, 20794-20799.
26. H. Gao, F. Xiao, C. B. Ching and H. Duan, *ACS Appl. Mater. Interfaces*, 2012, **4**, 2801-2810.
27. M. R. Karim, H. Shinoda, M. Nakai, K. Hatakeyama, H. Kamihata, T. Matsui, T. Taniguchi, M. Koinuma, K. Kuroiwa, M. Kurmoo, Y. Matsumoto and S. Hayami, *Adv. Funct. Mater.*, 2013, **23**, 323-332.
28. W. Zhang, M. Han, Z. Jiang, Y. Song, Z. Xie, Z. Xu and L. Zheng, *ChemPhysChem*, 2007, **8**, 2091-2095
29. H. Tang, G. J. Ehlert, Y. Lin and H. A. Sodano, *Nano lett.*, 2012, **12**, 84-90.
30. Y. Qi, H. Zhang, N. Du and D. Yang, *J. Mater. Chem. A*, 2013, **1**, 2337-2342.
31. J. Shu, R. Ma, L. Shao, M. Shui, D. Wang, K. Wu, N. Long and Y. Ren, *Electrochim. Acta*, 2013, **102**, 381-387.
32. C. Peng, B. Chen, Y. Qin, S. Yang, C. Li, Y. Zuo, S. Liu and J. Yang, *ACS Nano*, 2012, **6**, 1074-1081.
33. F. D. Wu and Y. Wang, *J. Mater. Chem.*, 2011, **21**, 6636-6641.
34. S. Laruelle, S. Grugeon, P. Poizot, M. Dollé, L. Dupont and J. M. Tarascon, *J. Electrochem. Soc.*, 2002, **149**, A627-A634.
35. L. Su, Z. Zhou and P. Shen, *Electrochim. Acta*, 2013, **87**, 180-185.
36. P. Poizot, S. Laruelle, S. Grugeon, L. Dupont and J. M. Tarascon, *Nature*, 2000, **407**, 496-499.
37. D. Pan, S. Wang, B. Zhao, M. Wu, H. Zhang, Y. Wang and Z. Jiao, *Chem. Mater.*, 2009, **21**, 3136-3142.
38. M. l. Dollé, P. Poizot, L. Dupont and J.-M. Tarascon, *Electrochem. Solid-State Lett.*, 2002, **5**, A18-A21.
39. P. Balaya, H. Li, L. Kienle and J. Maier, *Adv. Funct. Mater.*, 2003, **13**, 621-625.
40. R. Dedryvère, S. Laruelle, S. Grugeon, P. Poizot, D. Gonbeau and J. M. Tarascon, *Chem. Mater.*, 2004, **16**, 1056-1061.
41. W. Wei, S. Yang, H. Zhou, I. Lieberwirth, X. Feng and K. Mullen, *Adv. Mater.*, 2013, **25**, 2909-2914.
42. Z. S. Wu, W. Ren, L. Wen, L. Gao, J. Zhao, Z. Chen, G. Zhou, F. Li and H. M. Cheng, *ACS Nano*, 2010, **4**, 3187-3194.
43. G. Zhou, D.-W. Wang, F. Li, L. Zhang, N. Li, Z.-S. Wu, L. Wen, G. Q. Lu and H.-M. Cheng, *Chem. Mater.*, 2010, **22**, 5306-5313.

The table of contents entry

A novel graphene sheet-wrapped cobalt hydroxide chloride composite is synthesized as a long-life anode material for lithium ion battery *via* a facile one-pot *in situ* hydrothermal route.

ToC figure